Estimating Friction Modulation From the Ultrasonic Mechanical Impedance

Nicolas Huloux, Corentin Bernard, Michael Wiertlewski

Estimation of the Modulation of Friction from the Mechanical Impedance Variations

Nicolas Huloux, Corentin Bernard, and Michaël Wiertlewski *Member, IEEE*

Abstract—Ultrasonic surface-haptic touchscreens produce compelling tactile sensations directly on the users' fingertips. The tactile sensations stem from the modulation of friction produced by acoustic radiation pressure, which reduces the contact between the skin and the glass plate. During this process, some of the vibrations are partly absorbed by the tissues, resulting in a conspicuous change in the vibration amplitude of the plate upon contact with the finger, which manifests as a net change in the system mechanical impedance. In this study, we leverage the observable change of impedance to estimate the acoustic levitation and the frictional force. The self-sensing method utilizes a model of the first principles governing the physical interaction between the plate and the skin, which relies on multi-scale contact theory. The model accurately describes the experimental influence of the amplitude on the observed impedance (i.e., the amount of energy absorbed and reflected) and can be used to estimate the friction coefficient ($R^2 = 0.93$). These results provide additional evidence of the partial levitation mechanism at play in ultrasonic friction-modulation. This finding can be useful for designing energy-efficient devices and provide design suggestions for using ultrasonic impedance for self-sensing friction forces.

Index Terms—Ultrasonic friction-modulation, Squeeze-film, Tactile devices, Surface haptics, Biomechanics

1 Introduction

An effective method for attenuating the rattle of a vibrating object or cutting short the ringing of a bell is simply to place a finger on its surface. The compliance of the skin allows for contact to develop over a large area, creating a connection through which vibrations travel and are dissipated via viscoelastic losses. This viscoelastic behavior not only dampens vibrations in the frequency range of tactile and auditory stimulation but also extends to the ultrasonic regime. This behavior is particularly notable when interacting with surface haptic devices that use ultrasonic vibrations to modulate fingertip friction. The amplitude of these vibrations is generally attenuated by the presence of the finger, leading to a smaller dynamic range.

However, achieving a large dynamic range with these ultrasonic surface haptic devices is essential to provide notable stimuli to restore the tangibility of touchscreens. A large variation in friction triggered by the user's movement can produce the illusion of touching relief [1], [2], [3], texture [4], [5], [6] or even buttons [7], [8], [9]. Patterning the variation in friction has been shown to improve the speed and accuracy of the interaction with touchscreens [10], [11].

To achieve drastic changes in friction, ultrasonic surface-haptic devices oscillate with an amplitude of several micrometers owing to highly resonant glass plates being excited by stiff piezoelectric actuators. Because of the resonance, the dynamic behavior is influenced by contact with skin, which absorbs vibrations and shifts the resonant frequency of the system. When a plate is driven at resonance by the piezoelectric actuators, the added viscosity and inertia of skin reduce the amplitude and shift the phase of the plate motion [12]. However, this effect is also an opportunity to examine the complex coupling between tissues, air, and the plate. The mechanical properties of a fingertip around the excitation frequency can be estimated by comparing the complex-valued impedance of the plate with and without the presence of the finger [7], [8], [13], [14].

However, these measurements of the biomechanics of skin assume that the plate and the skin are in perfect contact. In reality, the interaction between the ultrasonic wave and the skin is quite complex and adds its own dynamics. The leading theory states that an acoustic vibration produces an acoustic radiation pressure that slightly levitates the skin off the plate, creating a gap [15]. In addition to levitation, the skin is forced into oscillation by the plate. During each oscillation, the gap closes, creating a cushion of air on which the tissues bounce [16].

Kaci et al. derived a method to estimate the acoustic force applied to the skin during the harmonic oscillation produced by piezoelectric actuators. They noted that the acoustic force increases linearly for low amplitudes of the ultrasonic vibration, but reaches an inflection point at amplitudes of a few micrometers [17]. This result suggests that the transmission of acoustic energy from the plate to the finger might be influenced by the amplitude of the stimulation. However, the model does not provide an estimation of the interfacial gap, which is correlated to the friction force.

To estimate the friction force from the impedance, we developed a new dynamic model, illustrated Fig. 1. This model considers the interplay between vibration and friction at the timescale of ultrasonic vibrations (i.e., $\approx$ 20 µs), to model the absorption, transmission, and reflection of the waves, as well as the longer timescale of the acoustic levitation (i.e., $\approx$ 1 ms). This multi-scale model can accurately predict the variation in the friction force and offers a unique view of latent variables such as the levitation gap.

- *N. Huloux is with Aix-Marseille Univ., CNRS, ISM, Marseille France*
- *C. Bernard is with the Perception Representation Image Sound, and Music laboratory, Aix-Marseille Univ., CNRS, Marseille, France.*
- *M. Wiertlewski is with TU Delft, Delft, The Netherlands. m.wiertlewski@tudelft.nl*

This research was supported by the Agence Nationale de la Recherche project IOTA ANR-16-CE33-0002

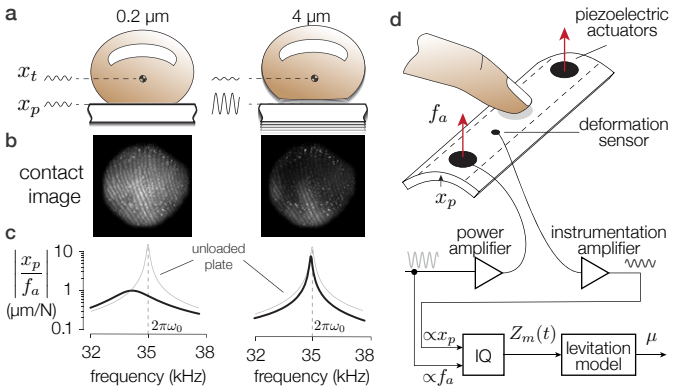

Fig. 1. **a**. Illustration of the motion of the skin and the plate at its anti-node. **b**. Frustrated total internal reflection imaging of the contact showing the decrease in the real contact area due to levitation [15]. **c**. Bode diagram of the admittance of the plate with the finger (black lines) compared to the plate without a load (gray lines). The influence of the finger is maximum for small amplitudes. **d**. Schematic of the fingertip interacting with the ultrasonic plate. The piezoelectric actuators produce a force, causing vibration of the plate. From these variables, the model first computes the plate impedance Z_m and then estimates the friction coefficient μ.

2 Related Works

2.1 Ultrasonic friction reduction theories

The first theories of ultrasonic friction modulation revolved around the principle of squeeze-film overpressure [2], [18]. Air is trapped between a vibrating plate and an idealized rigid and flat fingertip. Because of the vibration, the gap between the plate and the finger closes too quickly for the air to escape from the edges of the contact, therefore undergoing an isothermal compression cycle. The non-linear compressibility of air, modeled by Boyle's law, creates a net force on the skin. This model well explains the interaction between two flat and rigid surfaces [19]. An alternative to squeeze-film theory argues that the skin bounces on the plate, making intermittent contact of short duration, resulting in a reduction in the overall friction [20], [21]. Recent investigations under reduced pressure showed that air is nonetheless a critical factor in the modulation of friction [16], [22].

The rigid plate model is also a poor approximation of skin, which is both rough and compliant and therefore involves a range of physical phenomena. Instead of pure bouncing or pure levitation, the mechanism behind the reduction in friction seems to involve both squeeze-film levitation and intermittent contact at the micrometer scale [15]. The skin bounces on a film of air, resulting in an interfacial gap that monotonically grows with increasing amplitude. With larger interfacial gaps, fewer asperities of the skin are in intimate contact with the plate which contributes to lowering the friction force. However, none of these modeling approaches considered the dynamics of the plate. The current article models the bouncing and partial levitation of the skin, as well as their effect on the oscillation of the ultrasonic plate.

2.2 Biomechanics of the fingertip

The mechanical properties of skin have a significant effect on the susceptibility to ultrasonic friction reduction. Fingertips that are too elastic [14], [23] or that show a large overall impedance, i.e., large inertia and damping, tend to be unaffected by ultrasonic vibrations [8]. The mechanical behavior of skin has been extensively studied in the low-frequency end of the spectrum, where skin behaves mostly as an overdamped spring and damper system [24], [25], [26], [27] but little is known about the behavior in the ultrasonic range. Some models use a mass, spring, and damper series to capture the complex dynamics [28]. Recent measurements that rely on the self-sensing capabilities of ultrasonic friction modulation devices showed that skin behaves as a mass of ≈0.1 g in parallel with a damper of ≈20 N.s/m in the 30 to 40 kHz range [8]. At these frequencies, the elasticity of the tissues contributes insignificant forces and can be neglected.

2.3 Contact mechanics

The contact between the skin and the plate also strongly influences the levitation and therefore the behavior of the ultrasonic friction-modulation. In particular, the relationship between the force required to maintain both bodies in contact and the size of the gap is of utmost importance for modeling the dynamics. Skin is soft and rough; therefore, the contact between the plate and the fingertip is not as straightforward as the contact between two flat surfaces. The gross deformation of the fingertip as well as the contact with the fingerprints could be modeled by Hertzian contacts [29]. Doing so well captures the interaction at two spatial scales —the fingertip and the ridges— but fails to take into account the smaller-scale asperities that are affected by ultrasonic vibrations. Multi-scale contact theory provides a mathematical framework to model the interaction between two randomly rough surfaces. In this theory, the gap for a given force is predicted by the shape of the frequency spectrum of the roughness, itself modeled as a fractal surface, in which the Hurst exponent and the height distribution of asperities completely determine the contact state [30].

2.4 Mechanical Impedance

The plate and piezoelectric actuators create a dynamical system that has reactive elements –mass, spring, or capacitance– and dissipative elements in the form of dampers or resistors [13]. The amplitude and phase of the motion for the force produced by the actuators is a direct consequence of these parameters. To capture the dynamics of the system, it is useful to introduce the notion of impedance, which is a complex value that links the harmonic force to the harmonic velocity, generalizing the behavior of the reactive and dissipative lumped-elements. Similar methods in the electrical domain have led to an increased understanding of the electroadhesion of skin [31].

The real part of the impedance is related to the dissipative elements that decrease the overall energy of the system, and the imaginary part captures the behavior of the elements responsible for storing oscillatory energy. Common impedance values are: $Z \propto i\omega$ for an inertia, $Z \propto 1/i\omega$ for a spring, and $Z = cst$ for a damper, where $i = \sqrt{-1}$ is the imaginary number and ω is the angular frequency.

The mechanical impedance of the plate is found by dividing the complex-valued force produced by the piezoelectric elements by the complex-valued motion of the plate

using IQ-demodulation. When no finger is touching the plate, the impedance measurement reflects the dynamics of the plate itself and the dynamic behavior is changed with the contact of a fingertip. From the difference between the loaded and unloaded impedances, it is possible to recover the mechanical impedance of the skin, assuming that the skin is in total contact with the plate [8]. In this article, we relax this last assumption to estimate the biomechanics of the skin as well as the levitation height.

3 Modeling Contact Dynamics

The complex interaction between a finger and a vibrating plate is captured by a two-degree-of-freedom lumped parameter model. One of the degrees is related to the motion of the skin and the other to the motion of the plate. The elements of the soft tissues have the subscript t, and those concerning the behavior of the plate have the subscript p. Each of the parts is connected by a spring in parallel with a damper, which models the action of both the contact and the partial levitation indicated by the subscript c. The model is presented in Fig. 2a and b. Two external forces are applied to this system: f_e models the action from the finger motion and subsequently captures the slow behavior of the compression of the pulp and the levitation of the skin; f_a is the harmonic force provided by the piezoelectric actuators.

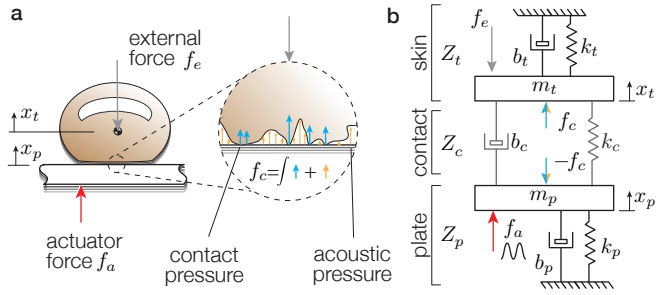

Fig. 2. **a**. Model of the interaction between the finger and the plate. The finger pushes on the vibrating plate. At the interface (inset) the force is split between the reaction force from the plate on the asperities of the skin and the squeeze-film pressure. The value of the latter is influenced by the nominal gap and the vibration amplitude. **b**. Two-degree-of-freedom model of the interaction. Around the ultrasonic excitation frequency, both the plate and the fingertip are modeled as a second-order mass-spring-damper system. A spring, which connects both bodies, lumps the interactions arising from the contact and partial levitation.

3.1 Constitutive equations

In the time domain, the free body diagram of the dynamic system, illustrated in Fig. 2, leads to the following equations:

$$\begin{aligned} m_t\,\ddot{x}_t + b_t\,\dot{x}_t + k_t\,x_t &= f_c - f_e \\ m_p\,\ddot{x}_p + b_p\,\dot{x}_p + k_p\,x_p &= -f_c + f_a \end{aligned} \tag{1}$$

where m_p, b_p, and k_p represent the mass, damping, and stiffness of the plate and m_t, b_t, and k_t represent the mass, damping, and stiffness of the fingertip tissues. The internal force f_c represents the forces at the contact between the finger and the plate, encapsulating the reaction force from the skin asperities and acoustic radiation pressure from the ultrasonic vibration. The connection between the plate and fingertip dynamic systems is modeled as a spring k_c in parallel with a damper b_c. This spring and the damper encapsulates the behavior of the asperities in contact and the squeeze-film levitation such that:

$$k_c\,(x_p - x_t) + b_c(\dot{x}_p - \dot{x}_t) = f_c \tag{2}$$

The constitutive equations are solved at two different timescales: at ultrasonic frequencies and at the quasi-static timescale. At the ultrasonic time scale, close to the period of oscillation of the plate, the motion follows a harmonic trajectory with zero mean and is indicated by a tilde $\tilde{\cdot}$. At the quasi-static time scale of the motion of the tissues, the forces and motions are equivalent to a time-averaged value, denoted with brackets $\langle\cdot\rangle$. Some variables, such as f_e, have only time-averaged values, whereas others such as f_a and x_p have only a harmonic component. Of particular importance, the contact force can be observed as the superposition of a time-averaged component and an oscillatory component:

$$f_c = \underbrace{\langle f_c \rangle}_{\text{time average}} + \underbrace{\tilde{f}_c}_{\text{harmonic}} \tag{3}$$

with $\langle f_c \rangle = \frac{1}{2\pi}\int_{-\pi}^{\pi} f_c \,\mathrm{d}(\omega t)$.

The model solves the constitutive equations, first in the harmonic regime and then at the quasi-static time scale, to derive a model of levitation that includes the dynamics of the tissues and the partial near-field levitation.

3.2 Harmonic behavior

Around the ultrasonic resonant frequency of the plate, the dynamic behavior is assumed to follow that of a second-order oscillator, and the system composed of Eq. 1 and Eq. 2 can be studied in the Fourier domain. The transformation to the Fourier domain is achieved by recognizing that the harmonic force produced by the actuator is $\tilde{f}_a = |\tilde{f}_a|\,e^{i\omega t}$, where t is the time variable, $i = \sqrt{-1}$ is the unit imaginary number and ω is the excitation frequency which corresponds to the natural resonant frequency of the unloaded plate in this article but can vary without loss of generality to accommodate situations where the frequency is regulated [32]. Since the external force is slowly varying compared to the ultrasonic oscillation, we can assume that it is constant such that $\tilde{f}_e = 0$. The respective harmonic velocities $v_\beta = \dot{x}_\beta$ of the skin and the plate are $\tilde{v}_\beta = |\tilde{v}_\beta|\,e^{i\omega t - i\phi_\beta}$ with $\beta = \{t, p\}$ and ϕ_β being the phase of the signal related to the actuator force.

Integrating and differentiating harmonic forces and displacements with respect to time leads to the expression of the constitutive equations in the Fourier domain:

$$\begin{aligned} \left(m_t\,i\omega + \frac{k_t}{i\omega} + b_t\right)\tilde{v}_t + \left(\frac{k_c}{i\omega} + b_c\right)(\tilde{v}_t - \tilde{v}_p) &= 0 \\ \left(m_p\,i\omega + \frac{k_p}{i\omega} + b_p\right)\tilde{v}_p + \left(\frac{k_c}{i\omega} + b_c\right)(\tilde{v}_p - \tilde{v}_t) &= \tilde{f}_a \end{aligned} \tag{4}$$

At the resonant frequency, the inertia and stiffness of the plate cancel each other such that $k_p - m_p\,\omega^2 = 0$; however, for generality, the remainder of the article includes

these terms. This linear set of complex-valued equations can be compactly written by expressing the impedance of each independent part taken in isolation. The isolated plate, tissues, and contact impedance are defined as:

$$Z_t(i\omega) = m_t i\omega + \frac{k_t}{i\omega} + b_t \tag{5}$$

$$Z_p(i\omega) = m_p i\omega + \frac{k_p}{i\omega} + b_p \tag{6}$$

$$Z_c(i\omega) = \frac{k_c}{i\omega} + b_c \tag{7}$$

In this scenario, the experimental value of the impedance of the plate $Z_p(i\omega)$ can be trivially determined by measuring its impedance when no finger is in contact with it. The remainder of the paper explains how to find the biomechanical impedance of the skin $Z_t(i\omega)$ and the impedance that models the dynamics of the contact $Z_c(i\omega)$.

Using this shorthand notation, the system of equations can be written in a matrix form:

$$\begin{pmatrix} Z_t + Z_c & -Z_c \\ -Z_c & Z_p + Z_c \end{pmatrix} \begin{pmatrix} \tilde{v}_t \\ \tilde{v}_p \end{pmatrix} = \begin{pmatrix} 0 \\ \tilde{f}_a \end{pmatrix} \tag{8}$$

Inverting the matrix, we recognize that the impedance observed via the ratio of the force generated by the actuator and the vibration of the plate is:

$$Z_m = \frac{\left|\tilde{f}_a\right|}{|\tilde{v}_p|} e^{i\phi_p} = Z_p + \frac{Z_t\, Z_c}{Z_t + Z_c} \tag{9}$$

This equation demonstrates that the impedance measured at the plate is the sum of the isolated impedance associated with the parallel association of the contact and the fingertip impedance. When the plate is completely decoupled from the finger, $Z_c = 0$, and the impedance observed from the vibration sensor is equal to the isolated impedance of the plate $Z_m = Z_p$. Conversely, when the contact is of infinite stiffness $Z_c = \infty$, the impedance measured at the level of the plate is the impedance of the plate in series with the impedance of the finger $Z_m = Z_p + Z_t$. This hypothesis of infinite contact stiffness is the basis of the method used in [8], [14] to find the impedance of a fingertip offline or during the interaction. The harmonic contact force at the interface $\tilde{f}_c$, derived in [17], can be recovered from:

$$\tilde{f}_c = \tilde{f}_a - Z_p\, \tilde{v}_p = (Z_m - Z_p)\, \tilde{v}_p \tag{10}$$

It is worth noting that since the impedance of the tissues is defined as $Z_t = \tilde{f}_c / \tilde{v}_t$, the particle velocity of the tissues can be found from:

$$\tilde{v}_t = \frac{Z_m - Z_p}{Z_t}\, \tilde{v}_p \tag{11}$$

In practice, our interest lies in finding a method for estimating the contact gap via the impedance of the contact Z_c. The latter can be found from the real-time measurement of the impedance Z_m after having determined estimates for the impedances of the unloaded plate Z_p and the tissues Z_t:

$$Z_c = \frac{(Z_m - Z_p)\, Z_t}{Z_t - Z_m + Z_p} \tag{12}$$

The last equation is completely determined if we consider that Z_m is found from the IQ demodulation of the actuation voltage, $\propto \tilde{f}_a$, of the vibration *pickup* sensor $\propto \tilde{v}_p$. The mechanical impedance of the plate Z_p can be found when the finger is not on the plate and the mechanical impedance of the skin Z_t can be found by assuming that $Z_c = \infty$ when the signal is small.

3.3 Effect of contact stiffness on measured impedance

The system is simulated using realistic parameters from the apparatus used in the following experimental section 4.1 to explore the effect of the contact stiffness on the measured impedance Z_m. In this context, the vibrating glass plate is chosen to have a resonant frequency of $f_0 = \omega\,/\,2\pi = 35$ kHz and an inertia of $m_p = 8$ g. Therefore, the equivalent stiffness, close to the resonant mode, is found to be $k_p = (2\pi f_0)^2\, m_p = 380$ N/µm. The damping value of the unloaded plate is taken to be $b_p = 7.01$ N.s/m, which leads to a quality factor of $Q \approx 250$. A fingertip with mass $m_t = 0.1$ g, a negligible stiffness and a damping $b_t = 32$ N.s/m is considered. These values are consistent with the apparatus and measurements detailed in [7].

Typical evolutions of the real and imaginary parts of Z_m, as well as the ratio of velocities $|\tilde{v}_t/\tilde{v}_p|$, are shown in Fig. 3, for $k_c = [0.1 - 100]$ N/µm. These simulations use the aforementioned numerical values in Eq. 9.

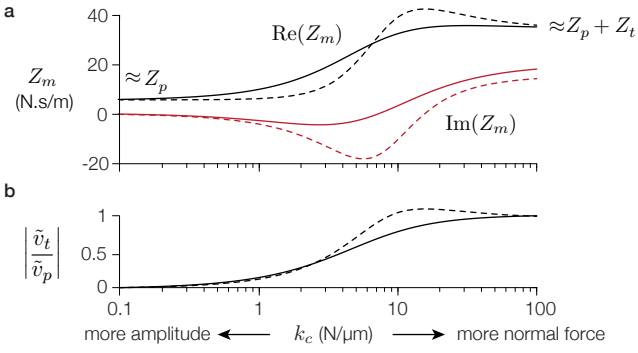

Fig. 3. Simulation of **a** the measured impedance of the plate and **b** the relative velocity between the skin and the plate, as a function of the contact stiffness. Dashed lines represent purely elastic coupling, and solid lines represent Kelvin-Voigt viscoelastic coupling with a damping factor of 0.3. At low contact stiffness, the skin decouples from the glass plate and the motion of the skin is almost null. Conversely, at high contact stiffness, the skin completely couples to the plate, and their velocities are equal.

The transmissibility of the vibration expressed by the ratio of the skin velocity to the plate velocity evolves between 0 for low contact stiffness and 1 for stiff coupling. Contact with a stiffness below 2 N/µm, which occurs for high vibration amplitudes, is soft enough that the impedance of the fingertip is barely reflected. Conversely, when the contact is fully formed and its stiffness greater than 5 N/µm, the observed impedance closely resembles the impedance of the plate and the impedance of the skin in series. At this level of coupling, the two impedances follow the same trajectory.

3.4 Time-averaged behavior

Thus far, we have seen that the contact stiffness k_c has a fundamental influence on the dynamic behavior of the system,

but the variables that influence its value are unclear. In this section, we seek to determine how the contact mechanics and acoustic levitation influence the contact stiffness.

At the interface between the plate and the skin, two main phenomena occur. First, only the highest asperities of the skin are in contact with the plate and support the interfacial load. Since the asperities are elastic, additional forces increase the number of asperities in contact. Second, the ultrasonic vibration of the plate creates an acoustic radiation pressure inside the air-filled gap where the skin is not in contact with the plate. Therefore, to model the contact stiffness, both phenomena need to be taken into account in the calculation, as illustrated in Fig. 4.

In the quasi-static analysis, we assume that the air trapped within the contact does not escape and is elastically compressed. This assumption results in no damping; however, some energy dissipation is likely to exist and contribute to the contact damping [33].

The contact forces are found by analyzing the dynamic system depicted in Fig. 2 at a slow timescale, where the ultrasonic vibrations are not considered individually but contribute to imposing a slowly varying levitation force f_s. At this timescale, the mean force coming from the actuator is null $\langle f_a \rangle = 0$ and only external pressure f_e is applied to the system. Therefore, the force balance at the contact simply becomes $\langle f_c \rangle = \langle f_e \rangle$, as shown in Fig. 4.

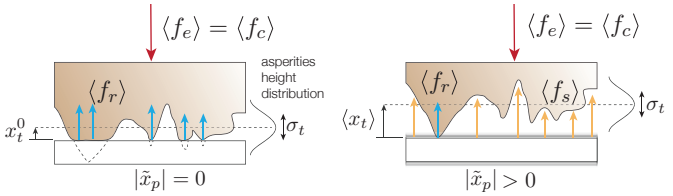

Fig. 4. Illustration of the interaction between the skin and the ultrasonic vibrating plate. The forces from the asperities in contact $\langle f_r \rangle$, squeeze-film levitation $\langle f_s \rangle$, and muscular activation $\langle f_e \rangle = \langle f_c \rangle$ are balanced. On the long timescale, the contact force f_c is only affected by the external load f_e. The fingertip roughness is modeled from multi-scale contact theory in which the height of the asperities follows a Gaussian distribution with a standard deviation σ_t and a mean x_t^0 at rest.

Following the development explained in the supplementary materials of [15], the contact forces $\langle f_c \rangle$ can be separated into the contribution of the acoustic radiation pressure forces $\langle f_s \rangle$ and the reaction force from the compression of the asperities of the skin $\langle f_r \rangle$ such that:

$$\langle f_c \rangle = \langle f_r \rangle + \langle f_s \rangle \tag{13}$$

Furthermore, an expression of the acoustic force is found by deriving the Reynolds lubrication equation in the gap between the finger and the plate such that:

$$\langle f_s \rangle = \frac{5}{4} p_0 \, S \frac{|\tilde{x}_p|^2}{\langle x_t \rangle^2} \tag{14}$$

where p_0 is atmospheric pressure and $S \approx 314$ mm^2 is the apparent contact area of a 20-mm diameter disc. The amplitude of the ultrasonic vibration acting on the plate is $|\tilde{x}_p|$, which is derived from $x_p = v_p/(i\omega) = |\tilde{x}_p| \, e^{i\omega t}$, previously defined in the harmonic analysis. Here, we set the time-average displacement of the plate to be null, i.e. $\langle x_p \rangle = 0$, so that the average gap between the two surfaces

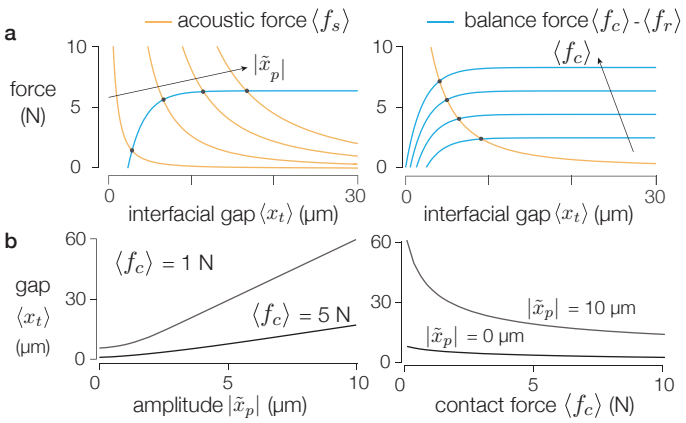

Fig. 5. **a**. Illustration of the contact equilibrium for various acoustic forces (left) and external forces (right). The dots correspond to the size of the gap at which the equilibrium between external forces, the acoustic radiation pressure, and forces on the asperities balance each other. **b**. Interfacial gap as a function of the amplitude and normal force.

$\langle x_t \rangle$ is the time-averaged position of the finger. The reader can refer to [15], [34] for more details on the derivation.

In addition to the force from acoustic pressure, the fingertip is also supported by the contact between the asperities and the glass surface. A relationship between the average gap and the reaction force can be found using multi-scale contact theory as follows:

$$\langle f_r \rangle = p_c \, S \exp\left(\frac{-\langle x_t \rangle}{\sigma_t}\right) \tag{15}$$

where $p_c = 0.375 \, q_0 \, \sigma_t \, E/(1-\nu^2)$ is the pressure coefficient that captures the elasticity of the asperities. This value is affected by the size of the asperity height distribution σ_t, the elastic properties of the material via the Young's modulus E and Poisson's ratio ν, and the length scale q_0 at which the measurements are made. See [15], [30] for more details on the derivation.

We can rewrite the equilibrium as a function of the initial average gap x_t^0 found in the absence of vibration. The previous equation can be rewritten as:

$$\langle f_r \rangle = \langle f_c \rangle \exp\left(\frac{-\langle x_t \rangle + x_t^0}{\sigma_t}\right) \tag{16}$$

where $x_t^0 = \sigma_t \ln(p_c \, S/\langle f_c \rangle)$ is the average gap formed by the contact in the absence of vibration.

Substituting 14 and 16 into the equilibrium Eq. 13 leads to:

$$\langle f_c \rangle \left[1 - \exp\left(\frac{-\langle x_t \rangle + x_t^0}{\sigma_t}\right)\right] = \frac{5}{4} p_0 S \frac{|\tilde{x}_p|^2}{\langle x_t \rangle^2} \tag{17}$$

Equation 17 is solved numerically (*vpasolve* in Matlab^{TM}) to find the levitation gap $\langle x_t \rangle$ that satisfies the force equilibrium. A representation of Eq. 17 for the roughness $\sigma_t = 2$ µm is given in Fig. 5a. Forces are shown as a function of the interfacial gap $\langle x_t \rangle$, solution of the equation for different contact forces $\langle f_c \rangle$ and amplitudes $|\tilde{x}_p|$. Equilibrium exists when reaction force $\langle f_r \rangle$ and acoustic force$\langle f_s \rangle$ are equal to the contact force, shown as dots in Fig. 5a. The effect of the vibration amplitude $|\tilde{x}_p|$ and the contact force $\langle f_c \rangle$ on the levitation gap is shown in Fig. 5b. Increasing the vibration

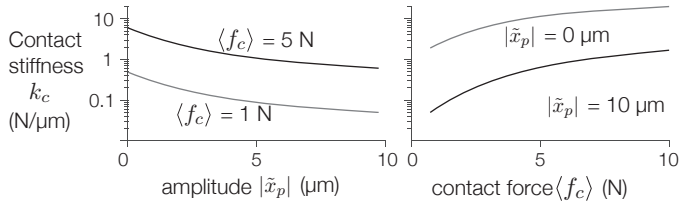

Fig. 6. Contact stiffness as a function of the vibration amplitude (left) and contact force (right)

amplitude leads to a larger gap, consistent with the partial levitation theory. Conversely, increasing the contact force closes the gap.

The contact stiffness can be found by taking the opposite of the gradient of the function that links the contact force to the gap, which we solved numerically, around the equilibrium point:

$$k_c = -\frac{\partial \langle f_r \rangle}{\partial \langle x_t \rangle} - \frac{\partial \langle f_s \rangle}{\partial \langle x_t \rangle} = \frac{\langle f_r \rangle}{\sigma_t} + 2\,\frac{\langle f_s \rangle}{\langle x_t \rangle} \tag{18}$$

The stiffness equation, illustrated in Fig. 6, makes it clear that as the gap between the skin and the plate increases, both the acoustic force and the reaction force from the asperities decrease, leading to a lower overall contact stiffness. In addition, regardless of the value of the external force, k_c asymptotically tends to 0 as the gap widens, leading to a decoupling of the finger from the plate for sufficiently high vibration amplitudes. When realistic fingertip parameters are used in the simulation, the contact stiffness is decreased by 90% for a 5 μm vibration amplitude and a 1 N external force.

3.5 Impedance and dynamics estimation

At this stage, we have a description of the influence of each impedance of the finger-plate system, as well as an estimate of the contact stiffness, which stems from the contact condition and the acoustic pressure. In this subsection, we connect both parts to build a forward model that relates the observed impedance Z_m to the vibration amplitude of the plate and the normal force applied by the user.

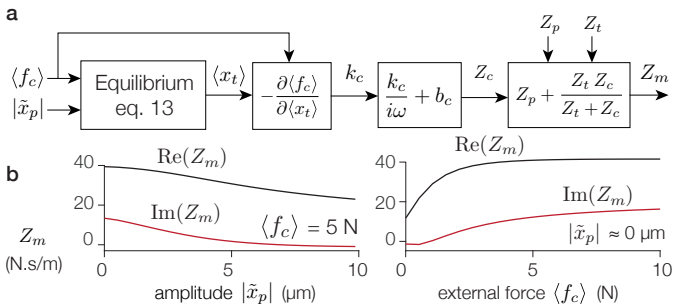

Fig. 7. **a**. Forward model that estimates the measured impedance from the external force and vibration amplitude. **b**. Estimation of the measured impedance at different external forces (left) and different vibration amplitude (right)

The measured impedance estimation process is represented by the block diagram in Fig. 7a. First, the time-averaged contact stiffness is estimated from the vibration amplitude and the external force. Then, assuming a viscoelastic compression of the contact asperities and the squeeze-film of air so that the contact impedance is $Z_c = k_c/i\omega + b_c$, the total impedance Z_m is computed from Eq. 9. The damping b_c is fixed following the Kelvin-Voigt viscoelastic coupling with a damping factor of 0.3, as it fits best the impedance measurements. The results for typical numerical values are shown in Fig. 7b.

Since both the acoustic and contact forces are monotonic, the function that expresses the levitation height at equilibrium as a function of the amplitude is also monotonic. This means that for a given set of the normal force and gap, a unique contact stiffness exists. In other words, it is possible to invert the relationship by using the contact stiffness found by the measurement to determine the value of the interfacial gap. This average interfacial gap has a direct influence on the friction force experienced when sliding.

Alternatively, the two-scale model can predict the levitation height and the amount of vibration transferred to the tissues, as illustrated in Fig. 8.

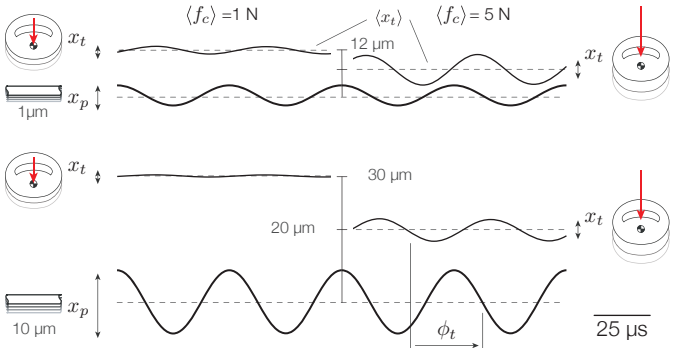

Fig. 8. Time-domain vibration of the plate and fingertip for two forces (1 N left and 5 N right) and two amplitudes (1 μm top row and 10 μm bottom row). The vibration of the skin decreases for the larger amplitude while the average height due to levitation increases.

The motion of the skin is found by solving the stiffness k_c and the average displacement $\langle x_t \rangle$ for a given set of the vibration amplitude and external force and then plugging the numerical values into the impedance equation. The harmonic part of the resulting complex-valued motion can be expressed as a magnitude and a phase such that $x_t = \tilde{x}_t\, e^{i\omega t - i\phi}$, where $\phi = \phi_t - \phi_p$ is the relative phase between the vibration of the plate and the vibration of the tissues.

The model predicts that large-amplitude vibrations of the plate increase the levitation height, which decreases the coupling between the skin and the plate and in turn reduces the transmission of vibrations to the tissues.

3.6 Friction coefficient estimation

The last step of the forward model is to connect the time-averaged interfacial gap $\langle x_t \rangle$ to the friction coefficient μ. Multi-scale contact theory, used to predict the levitation height, also provides a framework to predict variations in the friction coefficient.

As illustrated in Fig. 4, only the highest asperities of the skin contact the glass plate. If the external normal force decreases or the acoustic force increases, then fewer asperities will be in contact with the glass plate, creating a smaller real

contact area, which is composed of the contact area made by each individual asperity. As the average separation between the glass plate and the skin increases, fewer asperities are in contact and the ones that remain attached have a smaller individual contact area.

The adhesion theory of friction introduced by Bowden and Tabor [35], postulates that the friction force experienced by two tangentially sliding bodies is directly proportional to the real contact area. Therefore, a relative reduction in the contact area implies a relative reduction in the friction coefficient such that $A/A^0 = \mu/\mu_0$, where A_0 and μ_0 are the reference area and friction coefficient, respectively, which can be assessed when there is no vibration.

For a given normal force, the multi-scale contact theory can express the relative change in the real contact area and by extension of the friction coefficient, as a function of the average distance between the surfaces $\langle x_t \rangle$ such that:

$$\frac{\mu}{\mu_0} = \exp\left(\frac{-\langle x_t \rangle + x_t^0}{\sigma_t}\right) \tag{19}$$

As an example, the interfacial gap computed in section 3.4 can be used to estimate the contact friction coefficient as a function of the vibration amplitude, as shown in Fig. 9, with an initial friction coefficient of $\mu^0 = 0.8$ and a simulated fingertip roughness of $\sigma_t = 2$ µm under contact forces of 1 N and 5 N. As the amplitude increases, the levitation height rises, which reduces the friction coefficient to the point where the contact becomes almost frictionless.

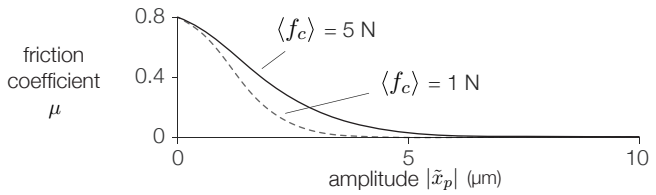

Fig. 9. Estimation of the friction coefficient from the multi-scale contact model as a function of the vibration amplitude for normal forces of 1 N (dashed) and 5 N (solid).

4 Experimental Validation

4.1 Apparatus

The experimental apparatus is depicted in Fig. 10. It comprises a $105 \times 22 \times 3.3$ mm^3 borosilicate glass plate, which is mounted on an aluminum holder by four nylon-tip screws pressing on the nodal line. The mount supports the quasi-static forces applied on the plate while allowing unimpeded vibratory motion. The plate undergoes flexural deformation along the 0×1 normal mode, which provides a constant amplitude across the length of the plate. For the excited mode, the boundary conditions of the entire plate are free. The modal mass corresponds to half of the actual mass, $m_p = 8$ g [13]. The plate stiffness is $k_p = (2\pi f_0)^2 m_p = 380$ N/µm, its internal damping is $b_p = \mathrm{Im}(f_a/\dot{x}_p) = 7.01$ N.s/m, and it has quality factor of $Q = \sqrt{k_p m_p}/b_p \approx 250$. The parameters for the second-order linear time-invariant model of the unloaded plate are identified by using a least-square fit to the admittance plot, expressed in the Fourier domain and shown in Fig. 10b. Two piezoelectric disks (SMD20T04, Steminc, Davenport, USA) are glued to the plate and provide excitation. The force delivered by the actuators is the product of the input voltage U_a applied to the electrodes and the force factor of the piezoelectric actuators glued to the plate γ. In practice, the force factor is found from the amplitude of the unloaded plate at resonance for a given voltage input, such as $\gamma = b_p\,\omega_0\,|x_p|/U_a = 0.13$ N/V. The wavelength of this mode is 22 mm, which is large enough to provide a comparable amplitude under the contact area.

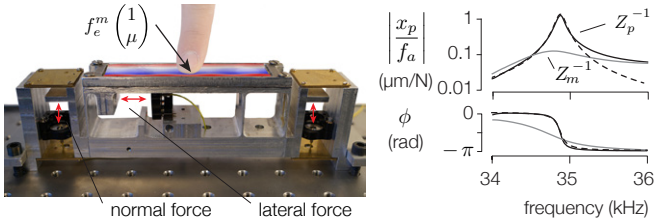

Fig. 10. **a**. Interferometric tribometer equipped with a resonating glass plate for friction modulation. The force is measured along with the lateral and normal directions. The vibration of the plate is shown in color; red indicates positive deformation and blue indicates negative deformation. The 1x0 mode is used so that the amplitude at the centerline of the plate is uniform. **b**. Typical measurements of the admittance Bode plot when the plate is unloaded (black) and when a finger is sliding (gray) represented by solid lines. The simulated plate admittance is shown in dashed lines.

The signal fed to the actuators is generated by a function generator (B&K Precision 4052, Yorba Linda, CA, USA) configured to produce an amplitude-modulated sine wave matching the resonant frequency of the glass plate, which appears at approximately 35 kHz. The signal is amplified $\times 20$ (WMA-100, Falco Systems, Katwijk, Netherlands). The deflection of the plate is measured by a third piezo-ceramic 5 mm-diameter disk which is sensitive to the deformation of the plate. The output of the piezoelectric pickup was calibrated with an interferometer (IDS 3010, Attocube, Munich, Germany) to measure the real-time vibration of the glass plate in micrometers. The input voltage into the piezoelectric actuators and plate vibrations were measured with an acquisition card (NI USB-6211 National Instruments) at a 100 kHz sampling rate, providing approximately 3 points per cycle. Lateral and normal forces imposed by the user on the plate were measured with the custom force sensor described in [36] and shown in Fig. 10 at a 10 kHz sampling rate.

4.2 Protocol

In total, 17 participants took part in the experiment, 5 females and 12 males, aged from 22 to 42 with a mean age of 28.2 years. The data of three participants were discarded due to technical issues. The participants were asked to explore the glass plate twice from left to right at a constant velocity of 50 mm/s by following a moving slider on a screen at a constant normal force between 0.5 and 0.8 N. At the end of each exploration, participants were informed of the average normal force they applied to help them self-regulate. The experiment received the approval of the ethics committee of the Aix-Marseille Université. The participants gave their informed consent before the start of the experiment.

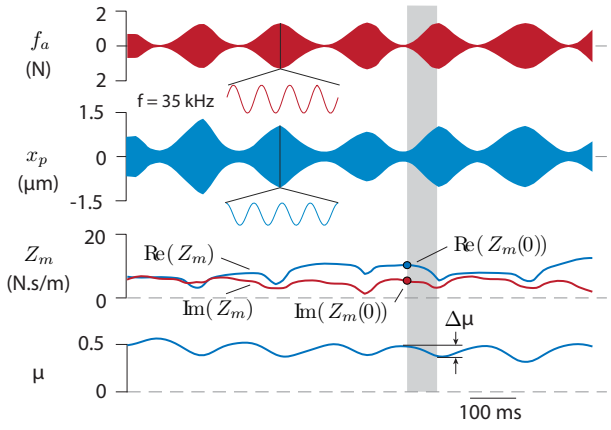

Fig. 11. Typical measurements of the plate vibration, impedance, and friction coefficient. The vibration amplitude is the carrier amplitude-modulated at 6 Hz modulated by the envelope $\tilde{x}_p$. The grey shading represents one instance of selected data.

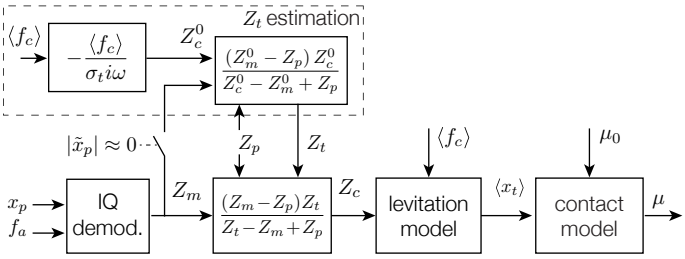

Fig. 12. The impedance Z_m is recovered from the IQ demodulation. The fingertip impedance Z_t is assumed to be constant during each trial and is found from the impedance at initial contact Z_c^0. Meanwhile, the contact stiffness for every vibration amplitude is recovered from its impedance estimation, Z_c. The interfacial gap $\langle x_t \rangle$ is then estimated from Z_c and $\langle f_c \rangle$. Lastly, the friction coefficient is estimated from Persson's model and initialized with the measured friction coefficient without vibration.

The friction was varied by the ultrasonic plate using an ultrasonic carrier, whose amplitude was modulated by a 6 Hz sine-wave with a modulation index of 95%. Typical measurements of forces and vibrations for one trial are presented in Fig. 11. The position of the finger was recorded with a pulley-encoder system, filtered with a second-order Butterworth filter with a 100 Hz cutoff frequency, and numerically differentiated to find the velocity. The dataset was further processed by selecting only instances where the finger was fully sliding with a constant velocity by cropping to sections of 60 mm at the center of the plate. Besides, because of the nonsymmetric behavior of friction reduction, only the sections where the friction force decreased were conserved (i.e., when the derivative of the vibration amplitude was positive). The resulting 60 ms force and impedance signals were then filtered with a second-order Butterworth filter with a 100 Hz cutoff frequency. Each trial is the compilation of 5 of these instances.

4.3 Mechanical impedance measurement

The instantaneous value of the mechanical impedance of the system, determined at the excitation frequency ($\approx$ 35 kHz for this device) is found by measuring the relative amplitude and phase of the vibration of the plate with respect to the actuation signal. The method to extract the mechanical impedance is described at length in the second half of [8] but the key aspects are concisely repeated here.

The impedance is found by taking the ratio of the analytical signals, so the first operation is to recover them from the measurements. The complex analytic representation of the plate deformation and the actuator forces is found by applying the Hilbert transform to the real-valued signals measured by the data acquisition board, denoted with the superscript m, such that:

$$\begin{aligned} \tilde{v}_p(t) &= v_p^m(t) + i\mathcal{H}(v_p^m(t)) \\ \tilde{f}_a(t) &= f_a^m(t) + i\mathcal{H}(f_a^m(t)) \end{aligned} \tag{20}$$

where $\mathcal{H}(\circ)$ denotes the Hilbert transform. The Hilbert transform of a monochromatic waveform is simply the same waveform that has been phase-shifted by 90°, recreating the missing imaginary part of the signal. This process essentially produces offline quadrature demodulation (also known as IQ demodulation) of the signals. Once the complex-valued analytic signals are recovered, the complex impedance of the plate-finger system is found using $Z_m(t) = \tilde{f}_a(t)/\tilde{v}_p(t)$, which provides a real-time estimate of the observed impedance, as shown in Fig. 11.

Snapshots of these real-time estimates in specific conditions are used to determine the isolated impedances of the system. The isolated impedance of the plate Z_p is obtained from the value of Z_m when the finger is not touching the plate and the plate can oscillate freely. Once the impedance of the plate is found, the impedance of the tissues Z_t is determined when the vibration amplitude is low enough. For low amplitudes, we can assume that the acoustic force is null and therefore find the initial contact stiffness Z_c^0 from Eq. 18. Once these values are found, the impedance of the tissues is computed from:

$$Z_t = \frac{(Z_m^0 - Z_p)\, Z_c^0}{Z_c^0 - Z_m^0 + Z_p} \tag{21}$$

In addition, the value of the impedance of the tissues is updated every time the vibration amplitude is below 0.2 μm, yet large enough so that force and velocity signals can be reliably measured.

The variation in the impedance of the contact is estimated from the measured impedance Z_m, once the impedances of the plate and the tissues are found. The impedance of the contact is later used to estimate the interfacial gap from the numerical solution of Eq. 18. Lastly, the friction coefficient is estimated from the gap using Eq. 19. The IQ demodulation provides an estimate of the impedance at all time steps. The initial parameters Z_t and μ_0 are, however, only calculated once for every cropped sequence and used throughout the sequence to determine the average gap and friction force from the impedance. The computational process to recover every metric is illustrated in Fig. 12.

4.4 Typical trial compared to numerical simulations

The results of processing a dataset of 5 isolated instances of a single typical subject over one exploration back and forth on the plate are shown in Fig. 13.

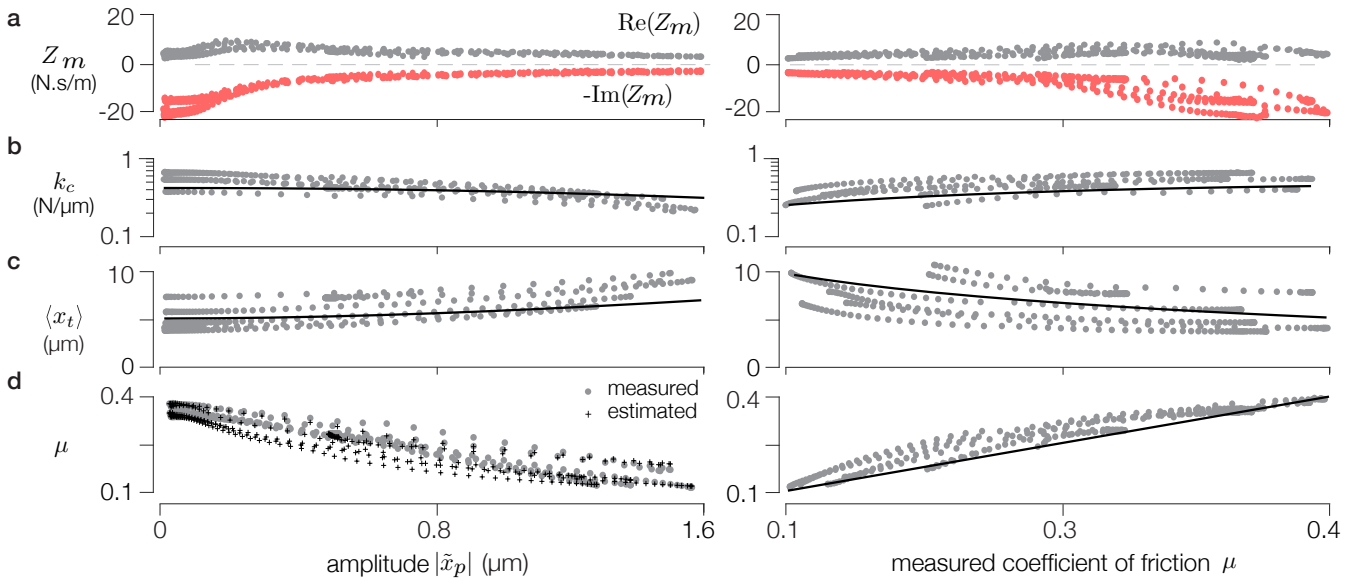

Fig. 13. **a**. Measured impedance Z_m for 5 typical instances of a finger sliding on an ultrasonic vibrating plate for a 0.5 N contact force. The opposite of the imaginary part is shown. **b**. Estimated contact stiffness. **c**. Estimated interfacial gap. **d**. Estimated friction coefficient (gray dots) and measured friction coefficient (gray crosses) as a function of the vibration amplitude (left) and its associated measured friction coefficient (right). Lines represent the latent variable of the model for this participant with fingertip roughness $\sigma_t = 1.7$ µm.

Fig. 13a shows that the real and imaginary parts of the measured impedance are initially close to 10 and 20 N.s/m, respectively, and both significantly decrease when the vibration amplitude is greater than 0.3 µm. The impedance asymptotically reaches the value of the impedance of the unloaded plate. The magnitude of this impedance is positively correlated with the friction coefficient for all trials (For all participants, Spearman's rank correlation is found to be $\rho = 0.78 \pm 0.26$, with $\rho = 0.73$ for the data in Fig. 13a).

The measurements were fitted with the results of the model predictions, where the average contact force of the trial and the measured vibration amplitude were used as input. The impedance of the fingertip Z_t and the initial coefficient of friction μ_0 were initialized when the amplitude was smaller than 0.2 µm. The estimated friction coefficient was then computed using the contact model. There was only one free parameter in the model: the fingertip roughness σ_t. The values of this parameter were found by minimizing the Euclidean distance between measured and estimated points using a Levenberg–Marquardt method over each selected instance. The Young's modulus and the contact area were fixed at $E = 20$ MPa and $S = 300$ mm^2 respectively, to make sure the optimization converged. For this particular dataset, the fitting procedure leads to $\sigma_t = 1.92 \pm 0.14$ µm. The model output using the averaged σ_t fits well the impedance data with $R^2 = 0.82$.

The contact stiffness, derived from the impedance variations, is shown Fig. 13b and follows the same downward trend with increasing amplitude. This trend is likely the result of levitation, which reduces the amount of coupling between the plate and the skin. The stiffness is positively correlated with the friction coefficient (in this particular case, the Spearman's rank correlation is $\rho = 0.91$), which is reasonable since they both depend on the true contact area created by the asperities. The interfacial gap, shown in Fig. 13c, is estimated from the contact stiffness. It increases with increasing vibration amplitude, which is consistent with the partial levitation theory. The variation in the friction coefficient is then estimated from the interfacial gap and follows the expected trend that the friction decreases for higher vibration amplitudes. The friction coefficient estimated from the variation in the measured impedance is shown alongside measurement in Fig. 13d and displays a similar trend, even if discrepancies exist. These discrepancies are likely due to variations in the biomechanics of skin and to roughness profiles that do not follow a Gaussian distribution. The discrepancies are larger for small amplitudes, which could result from the fluctuating behavior of the fingertip friction.

4.5 Results

The quality of the estimation of the friction coefficient from the impedance generalizes to the entire data set. The friction coefficient estimated with the impedance and the parametric model shows a remarkable correlation with the measured friction coefficient where Spearman's rank correlations are $\rho = 0.94 \pm 0.07$. To achieve a correct fit of the model and a robust estimation, trials for every individual subject were first fitted with parameters that converged to a value of roughness of $\sigma_t = 1.7 \pm 0.4$ µm. The relatively large inter-subject variability observed in the parameters is also found in the fingertip impedance Z_t, which averages to $Z_t = (0.47 \pm 0.28) + i\,(3.16 \pm 0.63)$ N.s/m.

The nominal value of the friction coefficient μ_0 is correlated to the imaginary part of the fingertip impedance Z_t over all trials (Spearman's rank correlation of $\rho = -0.58$, $\mathrm{p} = 10^{-11}$) and poorly to the real part ($\rho = -0.25$, $\mathrm{p} = 0.006$). However, the variation in the measured impedance (defined as the difference between the maximum and minimum value during one exploration) and the mea-

sured variation in the friction coefficient during every trial are significantly correlated (Spearman's rank correlation of $\rho = 0.58 \pm 0.27$ for the real part and $\rho = 0.65 \pm 0.3$ for the imaginary). This is most likely because during a single exploration, the biomechanical parameters do not change, as confirmed by the fact that the variations of the fingertip impedance Z_t are always less than 10% within a single trial.

The variation in the measured impedance $\Delta|Z_m|$ is slightly positively correlated with the variation in the friction coefficient $\Delta\mu$ (Spearman's rank correlation of $\rho = 0.28$ and $\mathrm{p} = 10^{-3}$), as shown in Fig. 14a. Interestingly, the acoustic force derived from this impedance via Eq. 10 has a moderately better correlation, with a Spearman's rank correlation of $\rho = 0.34$ ($\mathrm{p} = 10^{-3}$). The interfacial gap can be estimated from the value of the impedance, knowing the normal force applied by the participants. The variation in the interfacial gap $\Delta\langle x_t\rangle$ is correlated with the friction coefficient variation with a Spearman's correlation rank of $\rho = 0.43$ ($\mathrm{p} = 10^{-5}$).

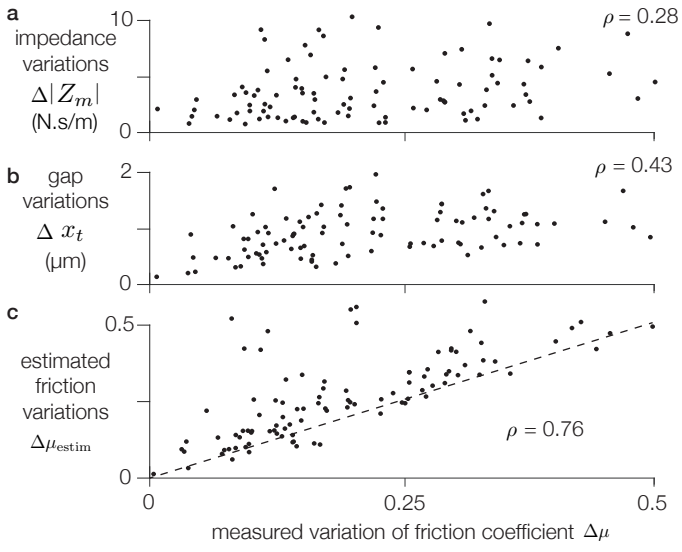

Fig. 14. Friction coefficient variation $\Delta\,\mu$ relation to the **a** measured impedance modulus $\Delta\,|Z_m|$, **b** estimated gap variation $\Delta\,\langle x_t\rangle$, and **c** estimated friction variation $\Delta\mu_{\mathrm{estim}}$. Points represent individual data of the 140 selected instances from the 14 subjects.

Furthermore, the estimated friction coefficient variation derived from the interfacial gap is presented in Fig. 14c. The 140 estimated friction variations show a linear positive correlation with the measured variation in friction (Pearson's correlation coefficient of $\rho = 0.76$, $\mathrm{p} = 10^{-20}$). However, the estimated variation is slightly over the measured one.

A scatter plot of each measurement and estimation of the friction coefficient is shown in Fig. 15. The initial value of the friction coefficient found when the amplitude is close to zero, is represented by black dots. The gray points show the subsequent estimation of the friction coefficient stemming from the variation of impedance. If the estimation was perfect, then every point would fall on the linear function with slope 1. While the estimation is short from perfect, the goodness of fit of the linear function is $R^2 = 0.98$, which demonstrates a relatively decent agreement between measurements and the short-horizon estimate from the impedance value.

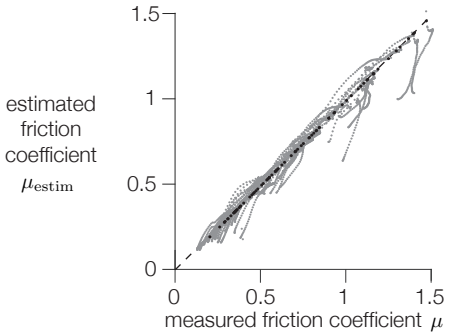

Fig. 15. Comparison of the estimated friction coefficient μ_{estim} and the measured friction coefficient, for all 140 trials. Black dots represent the initialization and gray dots are the subsequent predictions. The ideal linear function with slope 1, shown as a dashed line, has a goodness of fit of $R^2 = 0.98$.

5 Discussion

5.1 Ultrasonic energy transmitted to the skin

The levitation hypothesis of the friction modulation does not imply that the skin is stationary, quite the contrary. The model reveals that tissues undergo oscillatory motion at the same frequency as the vibration of the plate. Skin motion is more prominent when, first, the damping of the skin is low, as shown experimentally in [14], [23], second, when the vibration amplitude is small, and third, when the contact force is high. In realistic conditions, i.e., where the skin has a damping ratio above 0.5, the oscillations of the skin are out of phase with the ultrasonic motion, which is consistent with prior experimental findings [15]. The evidence suggests that the skin bounces on the squeeze-film of air.

This new analysis also raises questions about the actual value of the impedance of the skin measured at low vibration amplitude. Previous works used the assumption of an infinitely rigid contact at low vibration amplitude and assumed that the system impedance was equal to the fingertip impedance [7], [14]. However, this work introduces an additional stiffness and damping induced by the contact at the interface, which reveals a difference between the actual skin properties and the one measured with the assumption of perfectly rigid contact. Because of the dynamic coupling between the skin and the plate, we found that the fingertip impedance is most likely one order of magnitude lower than the measured system impedance.

Conversely, for extreme vibration amplitudes (i.e., above 5 μm), the model asymptotically predicts a complete decoupling of the plate and skin, which implies total levitation of the skin and the absence of intimate contact with the plate. Effectively the skin floats above the plate, supported by the action of the acoustic pressure.

5.2 Squeeze-film levitation and friction reduction

In addition to the oscillatory motion of the skin, this work shows that the time-averaged gap between the skin and the plate is strongly influenced by both the vibration amplitude and the force applied by the finger. According to multi-scale contact theory, this gap is directly related to the real contact area, created by summing the contributions of all the asperities in intimate contact with the glass plate [30].

According to the adhesive theory of friction, the real area of contact is related to the friction force via the shear strength of each asperity [37], creating a causal relationship between the gap, real contact area, and friction coefficient.

The experimental measure of the friction coefficient and its correlation with the estimated gap obtained by studying the variation in impedance confirm this prediction. To achieve levitation and open a gap between the skin and the plate, a large acoustic force is required. The correlation between the acoustic force and the friction force reported in [17] is also found in this work. The levitation force is derived from a linear combination of impedance measurements and therefore does not consider the state of the contact. Conversely, the estimate of the interfacial gap integrates both the information from the measured impedance and parameters such as the external force that play a role in the contact conditions. The comprehensiveness of the approach shows a better correlation with the levitation gap $\rho = 0.43$, than with the acoustic force, $\rho = 0.34$, in the current dataset. One cause of the discrepancy is that the acoustic force is partially lost to dissipation and might not be used to increase the gap, thus lowering the friction. The gap, on the other hand, has a causal and direct link to the friction coefficient, which might explain its lower variability.

5.3 Self-sensing of skin biotribology

Rendering precise and controlled stimuli on surface-haptic displays is not as elementary as controlling the force output of an electromagnetic motor. Because surface-haptic displays rely on the friction of the fingertip to create stimuli, the generation of the force is subject to high variability, owing to the complex tribological behavior of skin [37] and the inherent variability in the susceptibility to ultrasonic waves [8], [17]. This work proposes to examine the interaction that occurs at the interface between the skin and the plate, by estimating the impedance of the skin as well as the impedance of the interface itself.

The estimation of the friction coefficient from the model relies on the assumption that the fingertip impedance, skin Young's modulus, Poisson ratio, and the contact area are stationary during one exploration. In practice, these values can fluctuate, introducing additional variability that is not taken into account. However, more importantly, the frictional and adhesive properties of the skin are known to evolve with exploration speed and moisture [37], which might be the cause of discrepancies especially at amplitudes below 0.2 μm. The initial detachment of the skin might be impeded by viscous or adhesive forces at the interface. Another explanation of this discrepancy recognizes that when the vibration amplitude is low, noise in the impedance signal is likely to be more pronounced.

The biomechanics also play an important role in the perception of changes in friction [8], [38]. Softer or harder skin will experience more or less deformation of the tissues; as a consequence, the same vibration levels can lead to dramatic changes in the perception of the stimuli. Direct estimation of the impedance of the skin, which is now possible in this work, provides important information for shaping the input sent to a surface-haptic display and providing a consistent stimulus across users without adding additional force sensors to achieve closed-loop force feedback control [39], [40].

6 Conclusion

The vibration amplitude of an ultrasonic plate is significantly affected by the presence of a fingertip. In this article, we modeled the dynamic behavior of the plate and tissues via a lumped-element model, as well as a nonlinear model of the time-averaged behavior created by the partial levitation process. This model allowed us to examine the connection between the long time-scale (on the order of a second) capturing the motion of the skin imparted by the levitation and the ultrasonic time-scale in which we can model the dissipation and reflection of acoustic energy via the skin/plate measured impedance.

The main finding is that the higher the levitation of the skin is, the lower the coupling with the vibrating plate. This has two effects: first, the friction coefficient between the plate and the fingertip is reduced, and second, the plate vibrates more freely reducing the need for acoustic energy used to maintain the levitation. The model draws a comprehensive picture of the complex interconnection between the nonlinear process of squeeze-film levitation and the biomechanics of the tissues. The newfound understanding can serve to better control the tactile stimulation, not based on forces or the friction coefficient but on the easily measurable real-time impedance.

References

[1] L. Winfield, J. Glassmire, J. E. Colgate, and M. Peshkin, "T-pad: Tactile pattern display through variable friction reduction," in *Second Joint EuroHaptics Conference and Symposium on Haptic Interfaces for Virtual Environment and Teleoperator Systems (WHC'07)*. IEEE, 2007, pp. 421–426.

[2] M. Biet, F. Giraud, and B. Lemaire-Semail, "Squeeze film effect for the design of an ultrasonic tactile plate," *IEEE transactions on ultrasonics, ferroelectrics, and frequency control*, vol. 54, no. 12, pp. 2678–2688, 2007.

[3] C. Hudin, "Local friction modulation using non-radiating ultrasonic vibrations," in *2017 IEEE World Haptics Conference (WHC)*. IEEE, 2017, pp. 19–24.

[4] M. Amberg, F. Giraud, B. Semail, P. Olivo, G. Casiez, and N. Roussel, "Stimtac: a tactile input device with programmable friction," in *Proceedings of the 24th annual ACM symposium adjunct on User interface software and technology*. ACM, 2011, pp. 7–8.

[5] C. Bernard, J. Monnoyer, and M. Wiertlewski, "Harmonious textures: the perceptual dimensions of synthetic sinusoidal gratings," in *International Conference on Human Haptic Sensing and Touch Enabled Computer Applications*. Springer, 2018, pp. 685–695.

[6] M. K. Saleem, C. Yilmaz, and C. Basdogan, "Psychophysical evaluation of change in friction on an ultrasonically-actuated touchscreen," *IEEE transactions on haptics*, 2019.

[7] J. Monnoyer, E. Diaz, C. Bourdin, and M. Wiertlewski, "Optimal skin impedance promotes perception of ultrasonic switches," in *2017 IEEE World Haptics Conference (WHC)*. IEEE, 2017, pp. 130–135.

[8] ——, "Perception of ultrasonic switches involves large discontinuity of the mechanical impedance," *IEEE transactions on haptics*, vol. 11, no. 4, pp. 579–589, 2018.

[9] D. Gueorguiev, A. Kaci, M. Amberg, F. Giraud, and B. Lemaire-Semail, "Travelling ultrasonic wave enhances keyclick sensation," in *International Conference on Human Haptic Sensing and Touch Enabled Computer Applications*. Springer, 2018, pp. 302–312.

[10] V. Levesque, L. Oram, K. MacLean, A. Cockburn, N. D. Marchuk, D. Johnson, J. E. Colgate, and M. A. Peshkin, "Enhancing physicality in touch interaction with programmable friction," in *Proceedings of the SIGCHI Conference on Human Factors in Computing Systems*. ACM, 2011, pp. 2481–2490.

[11] G. Casiez, N. Roussel, R. Vanbelleghem, and F. Giraud, "Surfpad: riding towards targets on a squeeze film effect," in *Proceedings of the SIGCHI Conference on Human Factors in Computing Systems*. ACM, 2011, pp. 2491–2500.

[12] D. Ilssar and I. Bucher, "The effect of acoustically levitated objects on the dynamics of ultrasonic actuators," *Journal of Applied Physics*, vol. 121, no. 11, p. 114504, 2017.
[13] M. Wiertlewski and J. E. Colgate, "Power optimization of ultrasonic friction-modulation tactile interfaces," *IEEE transactions on haptics*, vol. 8, no. 1, pp. 43–53, 2014.
[14] R. F. Friesen, M. Wiertlewski, and J. E. Colgate, "The role of damping in ultrasonic friction reduction," in *2016 IEEE Haptics Symposium (HAPTICS)*. IEEE, 2016, pp. 167–172.
[15] M. Wiertlewski, R. F. Friesen, and J. E. Colgate, "Partial squeeze film levitation modulates fingertip friction," *Proceedings of the national academy of sciences*, vol. 113, no. 33, pp. 9210–9215, 2016.
[16] R. F. Friesen, M. Wiertlewski, M. A. Peshkin, and J. E. Colgate, "The contribution of air to ultrasonic friction reduction," in *2017 IEEE World Haptics Conference (WHC)*. IEEE, 2017, pp. 517–522.
[17] A. Kaci, A. Torres, F. Giraud, C. Giraud-Audine, M. Amberg, and B. Lemaire-Semail, "Fundamental acoustical finger force calculation for out-of-plane ultrasonic vibration and its correlation with friction reduction," in *2019 IEEE World Haptics Conference (WHC)*. IEEE, 2019, pp. 413–418.
[18] T. Watanabe and S. Fukui, "A method for controlling tactile sensation of surface roughness using ultrasonic vibration," in *Proceedings of 1995 IEEE International Conference on Robotics and Automation*, vol. 1. IEEE, 1995, pp. 1134–1139.
[19] E. Salbu, "Compressible squeeze films and squeeze bearings," *Journal of Basic Engineering*, vol. 86, no. 2, pp. 355–364, 1964.
[20] L. Winfield, J. Colgate, M. Lin, and M. Otaduy, "Variable friction haptic displays," *Haptic rendering: Foundations, algorithms and applications, MC Lin and M. Otaduy, Eds. AK Peters, Ltd*, 2008.
[21] E. Vezzoli, Z. Vidrih, V. Giamundo, B. Lemaire-Semail, F. Giraud, T. Rodic, D. Peric, and M. Adams, "Friction reduction through ultrasonic vibration part 1: Modelling intermittent contact," *IEEE transactions on haptics*, vol. 10, no. 2, pp. 196–207, 2017.
[22] W. B. Messaoud, E. Vezzoli, F. Giraud, and B. Lemaire-Semail, "Pressure dependence of friction modulation in ultrasonic devices," in *Work-in-Progress in World Haptics Conference (WHC)*, 2015.
[23] R. F. Friesen, M. Wiertlewski, M. A. Peshkin, and J. E. Colgate, "Bioinspired artificial fingertips that exhibit friction reduction when subjected to transverse ultrasonic vibrations," in *2015 IEEE World Haptics Conference (WHC)*. IEEE, 2015, pp. 208–213.
[24] C. Jamison, R. Marangoni, and A. Glaser, "Viscoelastic properties of soft tissue by discrete model characterization," *Journal of Biomechanics*, vol. 1, no. 1, pp. 33–46, 1968.
[25] D. L. Jindrich, Y. Zhou, T. Becker, and J. T. Dennerlein, "Non-linear viscoelastic models predict fingertip pulp force-displacement characteristics during voluntary tapping," *Journal of biomechanics*, vol. 36, no. 4, pp. 497–503, 2003.
[26] T. A. Kern and R. Werthschützky, "Studies of the mechanical impedance of the index finger in multiple dimensions," in *International Conference on Human Haptic Sensing and Touch Enabled Computer Applications*. Springer, 2008, pp. 175–180.
[27] M. Wiertlewski and V. Hayward, "Mechanical behavior of the fingertip in the range of frequencies and displacements relevant to touch," *Journal of biomechanics*, vol. 45, no. 11, pp. 1869–1874, 2012.
[28] F. Giraud, T. Hara, C. Giraud-Audine, M. Amberg, B. Lemaire-Semail, and M. Takasaki, "Evaluation of a friction reduction based haptic surface at high frequency," in *2018 IEEE Haptics Symposium (HAPTICS)*. IEEE, 2018, pp. 210–215.
[29] B. M. Dzidek, M. J. Adams, J. W. Andrews, Z. Zhang, and S. A. Johnson, "Contact mechanics of the human finger pad under compressive loads," *Journal of The Royal Society Interface*, vol. 14, no. 127, p. 20160935, 2017.
[30] B. Persson, "Relation between interfacial separation and load: a general theory of contact mechanics," *Physical review letters*, vol. 99, no. 12, p. 125502, 2007.
[31] C. D. Shultz, M. A. Peshkin, and J. E. Colgate, "On the electrical characterization of electroadhesive displays and the prominent interfacial gap impedance associated with sliding fingertips," in *2018 IEEE Haptics Symposium (HAPTICS)*. IEEE, 2018, pp. 151–157.
[32] W. B. Messaoud, F. Giraud, B. Lemaire-Semail, M. Amberg, and M.-A. Bueno, "Amplitude control of an ultrasonic vibration for a tactile stimulator," *IEEE/ASME Transactions on Mechatronics*, vol. 21, no. 3, pp. 1692–1701, 2016.
[33] W. Langlois, "Isothermal squeeze films," *Quarterly of Applied Mathematics*, vol. 20, no. 2, pp. 131–150, 1962.
[34] A. Minikes and I. Bucher, "Coupled dynamics of a squeeze-film levitated mass and a vibrating piezoelectric disc: numerical analysis and experimental study," *Journal of sound and vibration*, vol. 263, no. 2, pp. 241–268, 2003.
[35] F. P. Bowden, F. P. Bowden, and D. Tabor, *The friction and lubrication of solids*. Oxford university press, 1956, vol. 1.
[36] C. Bernard, S. Ystad, J. Monnoyer, and M. Wiertlewski, "Detection of friction-modulated textures is limited by vibrotactile sensitivity," *IEEE Transactions on Haptics*, 2020.
[37] S. M. Pasumarty, S. A. Johnson, S. A. Watson, and M. J. Adams, "Friction of the human finger pad: influence of moisture, occlusion and velocity," *Tribology Letters*, vol. 44, no. 2, p. 117, 2011.
[38] W. B. Messaoud, M.-A. Bueno, and B. Lemaire-Semail, "Relation between human perceived friction and finger friction characteristics," *Tribology International*, vol. 98, pp. 261–269, 2016.
[39] W. B. Messaoud, M. Amberg, B. Lemaire-Semail, F. Giraud, and M.-A. Bueno, "High fidelity closed loop controlled friction in smarttac tactile stimulator," in *2015 17th European Conference on Power Electronics and Applications (EPE'15 ECCE-Europe)*. IEEE, 2015, pp. 1–9.
[40] N. Huloux, J. Monnoyer, M. Boyron, and M. Wiertlewski, "Overcoming the variability of fingertip friction with surface-haptic force-feedback," in *International Conference on Human Haptic Sensing and Touch Enabled Computer Applications*. Springer, 2018, pp. 326–337.

Nicolas Huloux has obtained his engineering diploma from Grenoble-INP in 2016 in mechanical engineering with double accreditation in industrial design. He is now pursuing a Ph.D. degree in haptics at the Biorobotics group of the Institute for Movement Sciences (ISM) at the University Aix-Marseille. His research interests are the physics of skin-surface contact, their implications to human tactile perception, and the design of surface haptics interfaces. His work received the Best Student Paper award at the 2018 Eurohaptics conference in Pisa, Italy.

Corentin Bernard graduated from the Ecole Centrale de Marseille in 2017 and holds a Master's degree in acoustics from the Aix-Marseille Université. Since 2018, he is a doctoral student in the Groupe PSA and two laboratories at the University of Aix-Marseille: the Perception, Representations, Image, Sound and Music Laboratory (PRISM) and the Institute for Movement Sciences (ISM). He is interested in understanding how humans perceive audio haptic stimuli to drive the design of multimodal human-computer interfaces. His work has been nominated for Best Paper at the 2018 Eurohaptics conference in Pisa, Italy.

Michaël Wiertlewski is an Assistant Professor at the Cognitive Robotics Department of the TU Delft in the Netherlands. He obtained his Ph.D. degree at the Université Pierre et Marie Curie under the auspices of the Commissariat à l'Énergie Atomique (CEA-LIST) in Fontenay-aux-Roses, France. In 2012, he joined the Neuroscience and Robotics (NxR) lab at Northwestern University in Evanston, IL, USA where he studied the physics of ultrasonic friction-modulation. From 2015 to 2019, he was CNRS Chargé de Recherche at Aix-Marseille University. He received the Early Career Award from the Technical Committee on Haptics in 2017. His main research interests include the design of tactile interfaces, the physics of the skin/surface interaction, and tactile perception.